

Role of Point Defects in Enhancing the Conductivity of BiVO₄

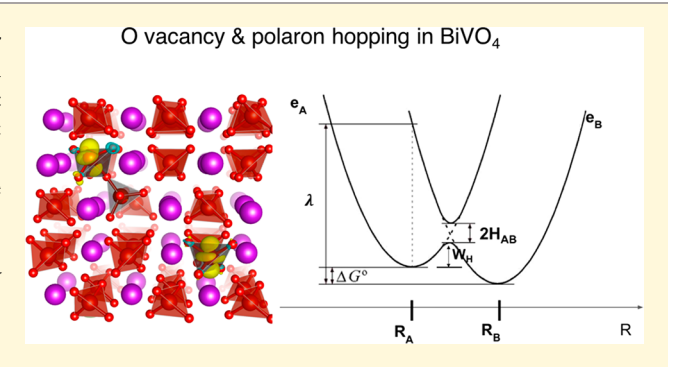
Hosung Seo, †,‡,§,⊥

Yuan Ping,†,||

and Giulia Galli*,§,⊥,#

Supporting Information

ABSTRACT: Bismuth vanadate is a promising photoanode for solar-to-fuel photocatalytic applications, and it has been extensively studied in recent years. However, the microscopic mechanism underlying the observed changes in electronic conductivity due to oxygen vacancies and nitrogen dopants remains unclear. Here, we combine electronic structure calculations at the hybrid density functional theory (DFT) level with constrained DFT, and we elucidate the role of defects in enhancing the transport properties of the material. We show that at low temperature, oxygen vacancies give rise to deep levels within the fundamental gap of BVO; however even as deep levels, oxygen vacancies can act as effective n-dopants and



polaronic charge carriers, due to their favorable position in energy relative to polarons in the pristine bulk. In addition, we show that N atoms can be easily introduced in n-doped BiVO₄ and that the presence of substitutional nitrogen affects the formation energy of polarons, effectively contributing to an increase of the carrier mobility in the material. Our results reconcile apparently conflicting experiments and they may be generalized to other transition metal oxides, thus providing a foundation for polaronic defect engineering in photoanodes for water photocatalysis.

1. INTRODUCTION

In recent years, BiVO₄ (BVO) has been identified as a promising photoanode to generate hydrogen fuel from water photocatalysis because of its several unique physical properties, 1-3 including efficient absorption of a substantial portion of the visible spectrum and a favorable position of its conduction band (CB) edge near the hydrogen evolution potential. Furthermore, a recent report showed that BVO photocorrosion during solar water splitting can be suppressed by tuning the composition of the electrolyte, thus improving the long-term photostability of the material⁴ In addition, the fast bulk and surface electron-hole recombination can be overcome by interfacing the light absorber with proper oxygen-evolution catalysts.

Despite the significant progress of the past few years in optimizing BVO for solar-fuel production, one fundamental problem remains: pristine BVO has extremely low intrinsic carrier conductivity⁵⁻⁷ and mobility (on the order of 0.1 cm² V^{-1} s⁻¹ for BVO compared, e.g., to 100–200 cm² V^{-1} s⁻¹ electron mobility for ZnO8), which constitute a major bottleneck for practical photocatalytic applications. Similar to other transition metal oxide (TMO) photoelectrodes such as Fe₂O₃ and CuO, the low carrier mobility of BVO is mainly attributed to its conduction mechanism dominated by thermally activated polaronic hopping, 9,10 much different from the fast band conduction characteristic, e.g., of III-V or IV semiconductors.

Several strategies have been proposed to improve the charge transport properties of BVO. 9-11 Previous studies reported that substitution of V with W, 9,10 Mo, 11 or P¹² (denoted as W_V , Mo_V , P_V), or substitution of O with N (denoted as N_O) could enhance the electron-hole separation and carrier conductivities. Intrinsic O vacancies (OV) have often been considered as shallow donors in BVO, 13 based on the results of Mott-Schottky measurements; hence increasing the OV concentration (for example, by H treatment) has been considered as responsible to improving the electron carrier concentration and hence the *n*-type conductivity in BVO.¹⁴ Hydrogen has also been extensively investigated as a potential n-type dopant. 15,16

However, the role of OVs in determining the electronic and transport properties of BVO and their interaction with impurities (such as H and N) are highly controversial, and as a consequence, the intrinsic n-type conductivity of the material remains largely unexplained. A recent experimental study 16 reported that hydrogen treatment improves the *n*-type

Received: July 28, 2018 Revised: September 26, 2018 Published: September 26, 2018

^{*}Department of Physics and Department of Energy Systems Research, Ajou University, Suwon, Gyeonggi 16499, Republic of Korea

[§]The Institute for Molecular Engineering, The University of Chicago, Chicago, Illinois 60615, United States

¹Materials Science Division, Argonne National Laboratory, Argonne, Illinois 60439, United States

Department of Chemistry and Biochemistry, University of California, Santa Cruz, California 95064, United States

Department of Chemistry, The University of Chicago, Chicago, Illinois 60615, United States

carrier concentration in BVO. However, OV concentration was unexpectedly found to decrease in the presence of H;¹⁷ in particular, upon annealing in the H2 atmosphere, Cooper et al. 16 observed a decrease of the intensity of a photoluminescence (PL) peak positioned ~0.6 eV below the conduction band edge, which was attributed to a decrease in OV concentration. Hence the increased carrier concentration could not be attributed to an increase in OV concentration, but rather it was interpreted as originating from H being a shallow donor passivating OVs. Cooper et al.'s data suggested since the states arising from OV are found to be ~0.6 eV below the conduction band edge (CBM), OV appears to be a "deep" defect with an ionization energy of ~0.6 eV to CBM, and hence an OV may not donate electrons at room temperature. Hence the authors concluded that it is H instead of OV that contributes to the n-type conductivity of BVO. However, ref. 17 showed that the electron carrier concentration increased in BVO after N₂ treatment and that N-treated BVO has an even higher carrier concentration compared to H-treated samples, a result which is not consistent with Cooper et al.'s claim. In addition to hydrogen, the interplay between OVs and N impurities was also shown to play a key role in determining the charge transport property of BVO. In a previous study, showed that both the carrier concentration and the mobility of BVO may be simultaneously enhanced upon N-doping. Our density functional theory (DFT) calculations showed that the formation of N-V bonds leads to the reduction of the static dielectric constant of the material, thus potentially lowering the hopping barriers for polaron transport. We previously described the hopping transport using a polaron model with parameters derived from DFT, implicitly adopting a continuum dielectric approximation, but we did not explicitly consider microscopic electron transfer processes.

The controversies present in the literature on the conduction mechanism of BVO (i.e., whether the presence OV increases the carrier concentration of BVO) call for a microscopic understanding of the fundamental role of OVs and of their interaction with intrinsic defects and impurities, such as N and H. Past DFT studies of intrinsic defects have been carried out using semilocal exchange-correlation functionals, which are inadequate to describe polaron formations in oxides due to charge delocalization errors. ^{18,19} For example, a puzzling negative ionization energy for OV (0/+2) in BVO was reported in a recent theoretical work, ¹³ which could be an artifact of using a semilocal functional. In addition, a microscopic understanding of polaron hopping rates in the presence of defects/dopants and of how these rates influence the macroscopic carrier mobility of the material is not yet available.

In this work, we present first-principles calculations using hybrid DFT and DFT+*U* combined with constrained DFT, aimed at describing the interplay between intrinsic and extrinsic defects and the formation of polarons in BVO. We examined the fundamental properties of OV and OV–N pairs, and we present a unified interpretation of several measurements, reconciling apparently conflicting experiments. We find that at low temperature OVs give rise to deep defect levels, relative to the pristine oxide conduction band maximum (CBM), which are however close in energy (within 0.1 eV) to that of the electron polaron in pristine BVO, implying that OVs can significantly contribute to the carrier concentration of *n*-type BVO by generating free polarons (i.e., electrons unbound to dopants). At room temperature, OVs levels are

expected to become shallower, based on recent theoretical investigations. ²⁰ In addition, we show that *n*-type BVO can be easily doped with N and that isolated N atoms may act as polaron "repulsion centers", thus possibly enhancing the mobility of charge carriers.

The rest of the paper is organized as follows. In section 2, we summarize the computational details of our hybrid DFT calculations of charged defects and of constrained DFT calculations of polaron transport. In section 3, we discuss our main results, including the transport properties of polarons in pristine and defective BVO, where OVs and N dopants are present. In section 4, we summarize the main implications of our results, with a focus on the role of the point defects in determining the conductivity of *n*-type BVO.

2. COMPUTATIONAL DETAILS

Using the Quantum Espresso code, 21 we carried out DFT and hybrid DFT calculations using plane-wave basis sets, and ONCV pseudopotentials 22,23 with a cutoff energy of 90 Ry. We used the dielectric-dependent hybrid (DDH) functional proposed in ref 24 with a Hartree–Fock mixing parameter $\alpha=0.145=1/\epsilon_{\infty}$, where the high-frequency dielectric constant ϵ_{∞} was set at 6.9, the value calculated in our previous study. We also carried out PBE+ $U_{\rm eff}$ calculations with only one effective parameter $U_{\rm eff}$ (= U-J). We applied $U_{\rm eff}$ (hereafter referred to as simply U) of 2.7 eV to the vanadium 3d manifold. In Table S1, we report the computed bulk properties of tetragonal ts-BVO and we discuss comparisons with experiment $^{26-30}$ and previous theoretical reports. Note that we considered the ts-BVO phase instead of the room-temperature monoclinic phase (ms-BVO) for simplicity, because we found that ts-BVO and ms-BVO have similar band structures and electron polaronic states. (see Figure 1). All polaron calculations in this study were performed including spin-polarization.

We considered OV, N impurities, and their pairs. To mimic the presence of isolated defects we employed a 3 \times 3 \times 1 (216-atom) supercell and we sampled the Brillouin zone with the Γ point only. We carried out numerical convergence tests as a function of supercell size, k-point sampling, and the plane-wave cutoff energy, and we found that the total energy obtained with a 216-atom supercell is converged within 2 meV/atom. All defect geometries were fully relaxed until the Hellman-Feynman forces were smaller than 10 meV/Å.

We investigated the defects' stability as a function of their charge state, by computing defect formation energies (DFE)³² $(E_{\rm f}^{D(q)})$ as a function of the Fermi level $(E_{\rm F})$:

$$E_{\rm f}^{D(q)}(E_{\rm F}) = E^{D(q)} - E^{H} - \sum_{i} n_{i} \mu_{i} + q(E_{\rm F} + E_{\rm V}) + E_{\rm corr}^{D}(q)$$
(1)

where $E^{D(q)}$ and E^H are the total energies of a supercell with and without a defect, respectively; μ_i (i = O, N) is the chemical potential and E_F is referred to the valence band edge (E_V). The term $E^D_{corr}(q)$ corrects for artificial electrostatic interactions arising in periodic supercell calculations, and was evaluated using the correction scheme developed by Freysoldt, Neugebauer, and Van de Walle³² with a static dielectric constant previously calculated ($\epsilon_0 = 52$).¹⁷

Because of a strong electron–phonon interaction in TMOs, electrons and holes usually form localized states accompanied by local lattice distortions, called polarons; $^{10,33-37}$ depending on their spatial extension, these are referred to as small or large polarons. Previous conductivity (σ) measurements of BVO as a function of temperature (T) point at a conduction mechanism arising from small polaron hopping above 250 K, and from a variable range hopping transport below 250 K. A distinct signature of polaron hopping conduction is the exponential dependence of σ on T: $\sigma \propto e^{-E_a/k_{\rm B}T}$, where $E_{\rm a}$ is the polaron hopping activation energy (or hopping barrier), and $k_{\rm B}$ is the Boltzmann constant. This behavior is markedly different from that of the carrier mobility in semiconductors,

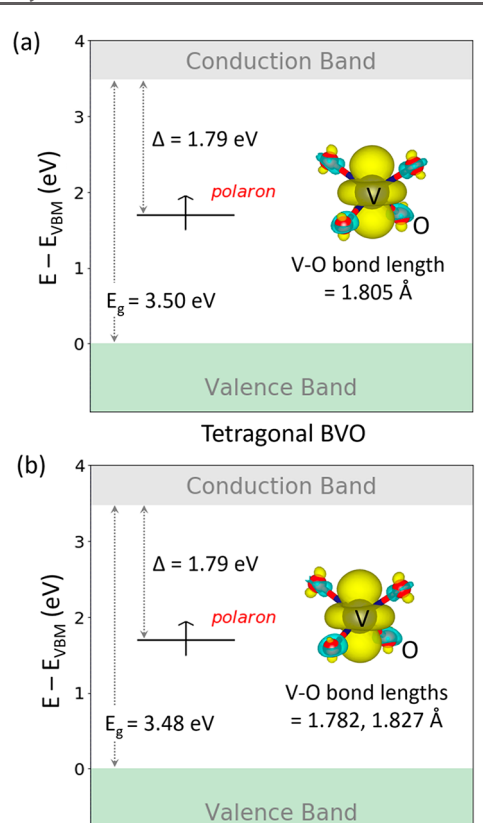


Figure 1. Electronic energy levels of (a) ts-BVO and (b) ms-BVO with one extra electron per supercell, computed using the DDH functional, at the respective experimental lattice constants. Insets show the square modulus of the electronic wave function associated with the polaronic state. The major difference between the two BVO phases is the presence of one single V–O bond length in ts-BVO, and two different V–O bond lengths in ms-BVO. In both phases, the polaronic state exhibits similar characteristics: a singly occupied nondispersive polaronic state is formed at 1.79 eV below the conduction band edge, with the same $3d_z^2$ orbital character; the band gaps differ by 0.02 eV in the two phases. The reason for the similarity is that the property of the electron polaron in BVO largely derived from the conduction band edge, i.e. the V 3d states, but the tetragonal

Monoclinic BVO

which originates from band conduction and decreases with increasing temperature, because of an increase in electron—phonon scattering.

to monoclinic structural distortion in BVO mainly affect the valence

band edge that is largely composed of O 2p, Bi 6s, and Bi 6p state.³

Small polaron transport in solids is typically described by the Landau—Zener theory (equivalent to the Emin-Holstein-Austin-Mott theory (EHAM) 34,36 in the context of the present application), with the associated parameters derived from quantum mechanical calculations. The polaron mobility (μ) is related to the charge transfer rates (τ) through the Einstein relation: $\mu = \frac{eD}{k_{\rm B}T} = \frac{eR^2n}{k_{\rm B}T}$, where D is the diffusion constant, R is the distance between two transfer sites, and n is the number of neighboring sites that can accept the electron transferred from a given donor site (note that this formula assumes isotropic hopping in three dimensions, within the weak electric field limit). The rate of charge transfer (τ) is given as $\tau = \kappa_{\rm el} \nu_n {\rm exp} \left(-\frac{W_{\rm H}}{k_{\rm B}T} \right)$, where $\kappa_{\rm el}$ is the electronic transmission coefficient, $\nu_{\rm n}$ is the effective frequency of the nuclear modes coupled to the electronic state; $W_{\rm H}$ is the hopping barrier for electron transfer (see Figure 2a) and is the main factor determining the carrier mobility, as it enters an exponential. In this work, we adopted a general formula for $W_{\rm H}$

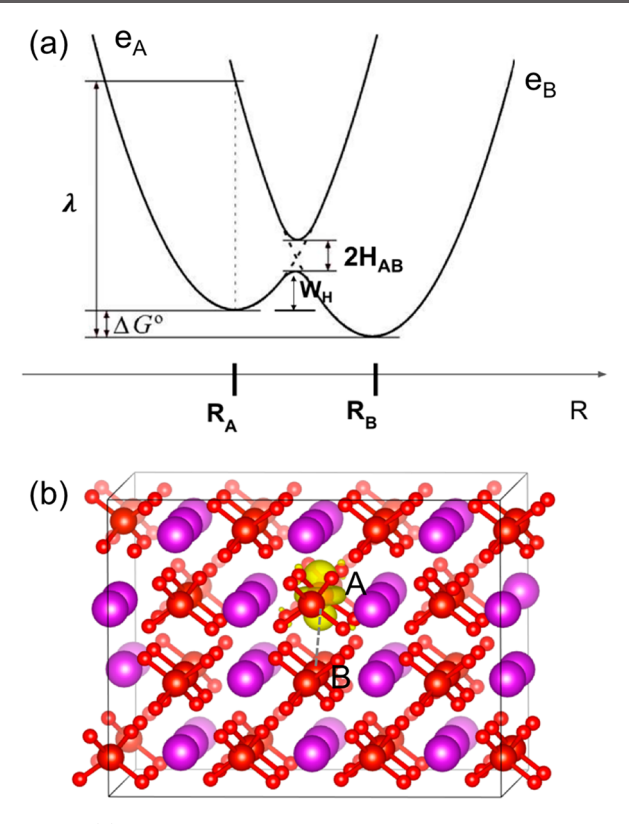


Figure 2. (a) Potential energy surface of polaron hopping from two different sites (A, B) of a BVO crystal, as a function of a configurational coordinate R. R_A and R_B correspond to donor and acceptor configurations, respectively. H_{AB} is the electronic coupling between the donor and acceptor, W_H is the activation energy or hopping barrier for electron transfer, λ is the reorganization energy, and ΔG^0 is the energy difference between the donor and acceptor states. e_A and e_B represent potential energy surfaces of electrons localized at A and B. (b) Ball and stick representation of a BVO crystal: the largest purple spheres represent Bi atoms, and the large and small red spheres represent V and O atoms, respectively. Nearest neighbor donor and acceptor sites are connected by a dotted gray line to guide the eye. The yellow isosurface represents the square modulus of the wave function of an electron trapped at site A and forming a polaron.

$$W_{\rm H} = \frac{(\lambda + \Delta G_{\rm o})^2}{4\lambda} - \left(|H_{\rm AB}| + \frac{\lambda + \Delta G_{\rm o}}{2} - \sqrt{\frac{(\lambda + \Delta G_{\rm o})^2}{4} + |H_{\rm AB}|^2} \right)$$

$$(2)$$

where $\Delta G_{\rm o}$ is the energy difference between the donor and acceptor states (see Figure 2a). Equation 2 is valid for both nonadiabatic and adiabatic hopping regimes. For example, when $H_{\rm AB}$ is vanishingly small, one recovers the nonadiabatic barrier: $W_{\rm H} = \frac{(\lambda + \Delta G_{\rm o})^2}{4\lambda}$ entering Marcus' theory.

To compute λ , $H_{\rm AB}$, $\Delta G_{\rm o}$, and $W_{\rm H}$ (see Figure 2a) in eq 2 from first principles, we used constrained DFT, as recently implemented for periodic systems. ⁴¹ In previous studies, energy barriers for polaronic hopping have only been computed for pristine systems (i.e., with no defects present), and with a linear interpolation (LE) method, ^{33,42} valid only in the adiabatic hopping regime. The LE method assumes that the transition state is located exactly on the linear extrapolated pathway between the initial and final states. In addition, previous CDFT calculations of reorganization energies, electronic couplings and charge transfer rates for polaron transport have employed finite-

cluster models that were assumed to represent a truncated portion of a bulk material. 35,43,444 Here we apply the CDFT method to supercell calculations, using periodic boundary conditions and, most importantly, our work is the first attempt to use CDFT to study polaron hopping in solids in the presence of defects.

3. RESULTS AND DISCUSSION

3.1. Electronic Structure of Pristine BiVO₄. We first considered the electronic properties of BVO in the absence of any defects and we investigated the formation of polarons in the system by adding an extra electron to the supercell (with a neutralizing background). The band structures of electron-doped BVO obtained with the DDH and PBE+U functionals are described in Figure S1. We find that the extra electron localizes as a small polaron at a V site, with the four nearest neighbors O^{2-} ions moving outward from the original V site by about 0.08 Å. The electronic wave function shows a predominant $3d_z^2$ character, with a strong coupling to the breathing mode of the VO₄ tetrahedron.

We computed the polaron hopping barrier W_H by CDFT (eq 2) using the DDH functional for pristine bulk BiVO₄. The electronic transfer energy diagram used in our calculations is shown in Figure 2. The donor configuration A is defined by constraining an electron at a V atom site (which has 4 nearest neighboring O²⁻ ions). The acceptor configuration B is defined by constraining an electron at a neighboring VO₄ unit as shown in Figure 2b. Using this donor-acceptor configuration, we found $W_{\rm H}$ = 0.24 eV (with the computed $H_{\rm ab}$ = 0.11 eV and λ 1.35 eV), a value smaller than the one (0.35 eV) obtained using the LE method and the HSE hybrid functional (α = 0.15),⁴² but closer to the measured polaron barrier (0.29 eV) in lightly doped BVO. 10 Note that the calculations carried out with eq 2 do not need to assume whether the hopping process is adiabatic or nonadiabatic; the LE method is instead only valid for an adiabatic process. In addition, LE does not locate the exact transition state for an adiabatic process, which may lead to an overestimate of the barrier.3

We remark that the computed hopping barrier is highly sensitive to the chosen exchange-correlation functional. Irrespective of the functional used, the charge difference between the donor and acceptor is constrained to have the same value; however, the decay of the wave function (which determines $H_{\rm AB}$) and the ionic and electronic polarizations of the environment (which determine the reorganization energy λ) turn out to be functional-dependent. For example, when using PBE, we obtained a negative barrier ($W_{\rm H} < 0$), which yields an incorrect band transport picture in BVO, at variance with the measured temperature dependence of the mobility.

3.2. O Vacancy and Electron Trapping. Oxygen vacancies are usually considered to be *n*-type dopants in oxides; the removal of an oxygen atom amounts to donating two electrons per vacancy, which have long been regarded as responsible for the intrinsic *n*-type conductivity of BVO. However, recent PL measurements suggested that the states induced by OVs may be rather deep with respect to the CBM of the material, ¹⁶ casting doubts on whether OVs are effective *n*-type dopants in BVO. We show below that the energy levels of the extra electrons donated by OVs are deep levels in the electronic gap, consistent with the findings of Cooper et al., ¹⁶ however, these levels can act as a source of polaronic charge carriers in the material, making OVs effective *n*-type dopants.

In order to understand the electronic states induced by OVs, we compared the total energy of several possible states of a neutral OV in Figure 3, and we divided them into two groups: vacancy-trapped electronic states, where electrons are localized

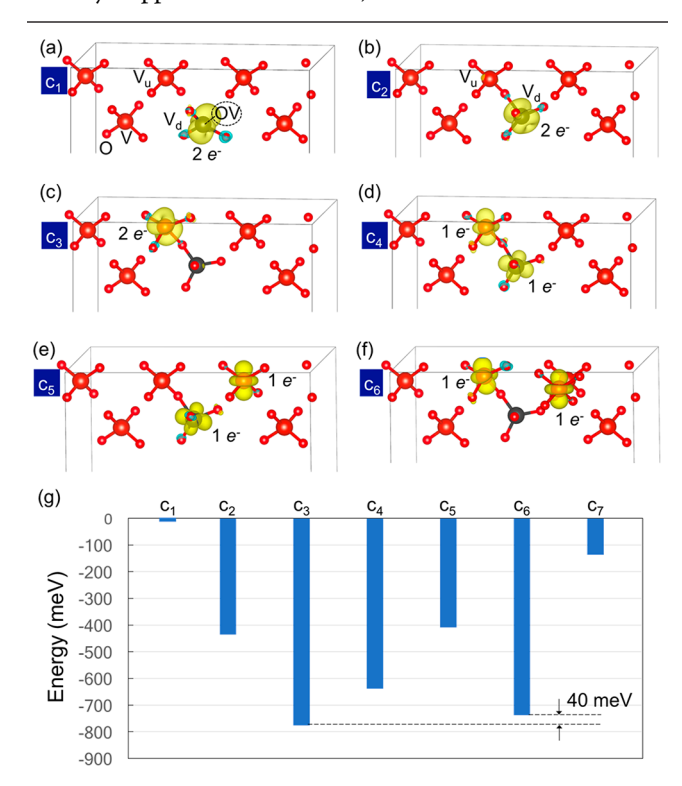


Figure 3. (a-f) Several configurations of electrons localized near an oxygen vacancy (OV) in BVO and (g) corresponding total energies of the defect states computed using the DDH functional. Vanadium and oxygen atoms are represented by large and small red spheres, respectively. Bi atoms and some of the VO₄ tetrahedra are omitted for clarity. (a) Two electrons originating from the OV (represented by a dotted sphere) are localized at a V atom site (labeled as V_d and represented by a black sphere) in the O-deficient VO₃ unit. (b-f) OV configurations where the O-deficient VO3 unit has a nearly VO4 tetrahedral geometry, where one O ion is shared with a nearest neighboring VO₄ unit whose V atom is labeled as V₁₁. The two extra electrons donated by the OV can be both trapped at the (b) V_d site or (c) the V_u site, or (d) one in each of the V_d and V_u sites. In these calculations, triplet spin configurations (S = 1) are considered. See Figure S2a, b for a discussion on the potential presence of singlet spin (S = 0) configurations. We also show configurations where one of the two electrons leaves the OV site and forms a small polaron in the bulk region of BVO, whereas the other electron is trapped at (e) V_d o (f)r V_u. (g) Diagram in which total energies are referred to that of the c1 configuration. The c7 configuration (its graphical representation is not shown in this figure) is one where both of the two extra electrons leave the OV site and forms small polarons in the bulk region of BVO. Figure S2c presents corresponding results obtained with PBE+U, showing qualitatively similar results.

at the OV site (configurations c1 to c4 in Figure 3g) and bulk polaronic states, in which one or both of the two extra electrons form small polarons in the bulk region of BVO, thus contributing charge carriers to the material (configurations c5 to c7 in Figure 3g).

In the vacancy-trapped electronic configurations (c1, c2, c3, and c4) shown in Figure 3a–d, the two extra electrons are localized in proximity of V sites neighboring the OV: in c1 the two electrons are localized in a VO_3 unit where an oxygen atom has been removed (denoted as V_d); in c2 the electrons are localized in V_d , where the geometry of the VO_3 unit is

modified in such a way as to share a corner with a neighboring VO_4 unit (denoted as V_u), thus effectively recovering a VO_4 stoichiometry; in c3, the two electrons are localized in V_u ; finally in c4, one electron is localized in V_u and the other one in V_d . As shown in Figure 3g, we find that c3 is the lowest-energy configuration.

In Figure 3e, f, we also considered two configurations (c5 and c6) where one electron is localized in proximity of the OV site (either V_u or V_d), but one is in the bulk region, away from the vacancy site. The important result shown by our total energy calculations is that configurations with two electrons trapped by the OV (c3), and configurations where one electron forms a small polaron in the bulk region (c6), are very close in energy. In particular, the energy difference between c3 and c6 (see Figure 3g) is found to be only 40 (140) meV, when using the DDH (PBE+U) functional. To double-check these energy differences, we also considered five more c6-like polaron configurations, which are shown in Figure S3. We found that the averaged energy difference is 42 (133) meV using the DDH (PBE+U) functional, which is consistent with the c3 and c6 energy difference in Figure 3(g). We note that this energy difference corresponds to the energy required to extract one electron from the OV site to the bulk region of the material, where it can act as a polaronic carrier. In other words, the ionization energy of one of the localized electrons is relatively small and at the finite temperature, it is likely for electrons localized at vacancies to become polaronic charge carriers.

To have a complete picture of OVs in terms of their charge state stability and ionization energy, in Figure 4 we report the defect formation energy (DFE) of the OV as a function of the Fermi level, calculated at the DDH level of theory (see Figure S5 for PBE+U results, which are qualitatively similar). We found that an OV may exhibit +2, + 1 and neutral states, positioned in energy within the band gap of BVO, with the (+1/0) and (+1/+2) charge transition levels (CTLs) at 0.76 eV (0.59 eV) and 1.14 eV (0.87 eV) below the CBM, respectively, at the DDH (PBE+U) level of theory. These results indicate that the ionization energy of the OV is 0.76 eV, which thus results to be a deep defect level. We also compared the (+1/0) CTL to the (0/-1) CTL of a single polaron in bulk BVO and we found that the ionization energy of the neutral OV with respect to the polaron level is 0.11 (0.21) eV using the DDH (PBE+U) functional; these results are consistent with those obtained from total energy calculations (0.04 and 0.14 eV, respectively, see Figure 3g). Hence, consistently, total energy differences and eigenvalue diagrams, show that OVs can act as single donors in BVO at finite temperature, in spite of electrons forming deep levels in the electronic gap of the material.

3.3. N Doping of BiVO₄. We now turn to the discussion of the effect of N doping and the interaction of N with OVs. Previous studies 17 indicated that in BVO N impurities play an important role in improving the conductivity when they coexist with OVs. We note that there are two possible cases: N substitutes for O (N_O), and N and OV form a defect complex (N_O-OV). In what follows, we separately examine the energetics of the N_O defect and the OV–N_O complex, followed by a discussion of their effects on the conductivity of BVO.

The computed DFE of $N_{\rm O}$ is reported in Figure 4. In most of the band gap region, the most stable state of $N_{\rm O}$ is negatively charged, indicating that N^{3-} , the natural ionic state

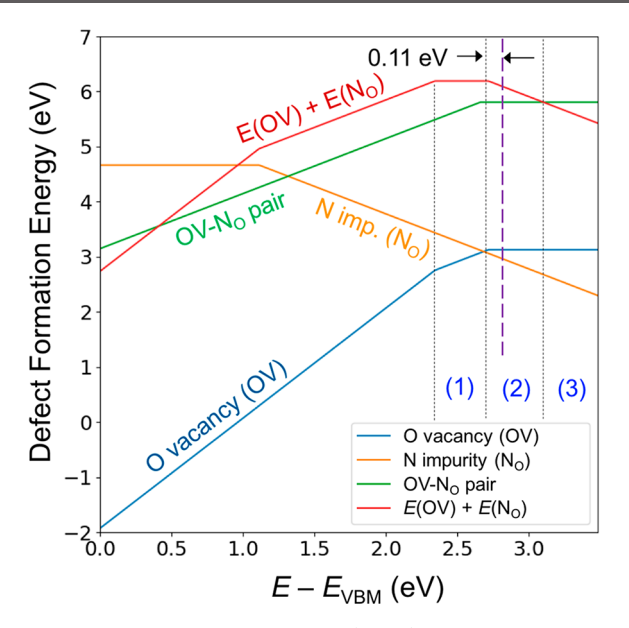


Figure 4. Defect formation energies (DFEs) of an oxygen vacancy (OV), a substitutional nitrogen (N_O) , and an OV- N_O pair in BVO in the O-rich limit, calculated using the DDH functional. The DFE is calculated as a function of the Fermi level (E) from the valence band maximum (VBM, E_{VBM}) to the CBM. There are three distinct regions of stability for OV and OV-No pairs, near the CBM, denoted as (1), (2), and (3) (see text). The figure shows the lowest energy configurations for all defects and all charge states. Some of the metastable states (higher in energy) found in our calculations are reported in the Supporting Information (e.g., see Figure S4 for a positively charged OV). The slope of a DFE line corresponds to the charge state of the defect, and the position of the Fermi level where two different charge states intersect yields the charge transition level (CTL, see eq 1 and Table S2.). The energy difference between the (+1/0) CTL of the OV (black, vertical, dotted line dividing the area (1) and (2)) and the CBM defines the ionization energy of the neutral OV with respect to the CBM. The vertical, purple, dashed line indicates the polaron level in BVO and the difference between this line and the (+1/0) CTL of the OV is calculated to be 0.11 eV; this energy corresponds to the ionization energy of the neutral OV with respect to the polaron level.

of N, is favored. Our previous study showed that neutral N induces a singly unoccupied defect state in the band gap of the material. We show here that this neutral defect state is stable when the Fermi level is located within $\sim 1.1~{\rm eV}$ from the valence band edge (i.e., below the (0/-1) CTL as calculated using the DDH functional). Above the (0/-1) CTL, the single N-induced defect state is occupied, and the negatively charged N impurity is stable. The square modulus of the wave function associated with the occupied N-induced defect state is presented in Figure S6, showing that the extra electron is mostly localized at the N ion site.

In addition to the substitutional N, we also considered interstitial N (N_i). We calculated its DFE at the DFT+U level of theory, which is reported in Figure S5. Focusing on the n-type region near the conduction band edge, we found that the DFE of N_i is higher than that of a substitutional N by more than 0.3 eV. Furthermore, N doping in BVO normally creates O vacancies at the same time. The DFE plot in Figure S5 also shows that if both N_i and OV are present and close to each other, it is energetically favorable to form N_O by combining N_i and OV in the n-type region; the DFE of N_O is smaller by \sim 3 eV than the sum of the DFE of OV and the DFE of N_i . Thus, it

is likely that the dominant form of the N impurity in BVO is $N_{\rm O}$, instead of $N_{\rm i}$. We note, however, that at a high temperature (e.g., 350 °C or higher), there could be an extra entropic contribution to the DFE that could potentially change the relative concentration of $N_{\rm O}$ and $N_{\rm i}$; the calculation of such contribution is beyond the scope of this study. In what follows, we only consider $N_{\rm O}$ unless stated otherwise.

When N_O and OV are close to each other, they may form an OV- N_O defect complex. To investigate the stability of such complex, we report in Figure 5 its total energy as a function of

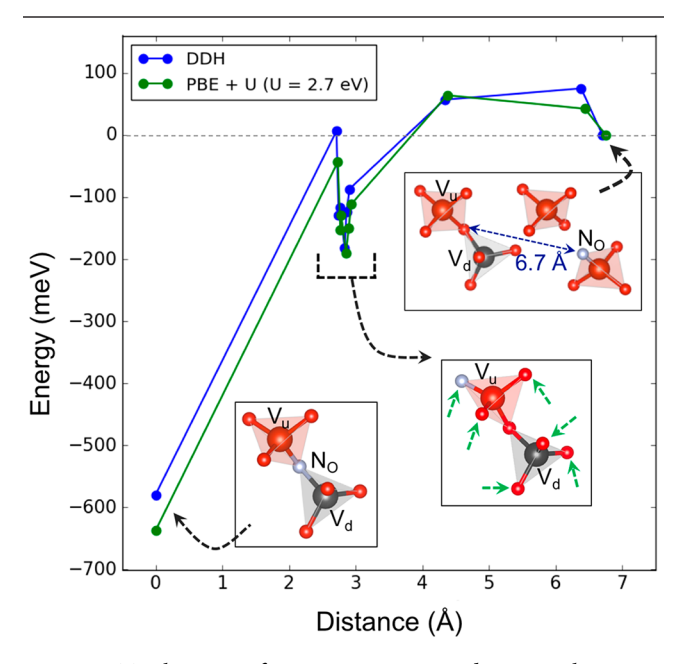


Figure 5. Total energy of an oxygen vacancy-substitutional nitrogen $(OV-N_O)$ pair as a function of the distance between OV and N_O , performed in a positively charged (q=+1) supercell, calculated using the DDH (blue dots) and the DFT+U (green dots) functionals. Results for other charged states are reported in Figure S7, showing similar trends. The calculations were performed using a single supercell, but with the N dopant and the O vacancy in different locations. The midpoint of the corner-sharing VO_4 tetrahedra where the OV is located is defined to be the origin. The energy of the configuration with N_O is the farthest apart from the origin is the zero of energy. The two lower panels show N_O located in the midpoint (left) and at one of the other 6 oxygen sites of the corner-sharing VO_4 tetrahedra (right), as indicated by green arrows. The upper panel shows the reference zero energy structure. The color code is the same as in Figure 3.

the distance between the vacancy and the dopant, for the positively charged state (created by removing one electron from the supercell, thus q=+1). The results for q=0 are reported in Figure S7. We found that the lowest-energy structure corresponds to the $N_{\rm O}$ dopant located at the cornersharing position of the VO₄ tetrahedra for the +1 and 0 charged states (see the Supporting Information).

The DFE of the OV-No complex is shown in Figure 4. We found that in most of the band gap region, the stable defect complex is positively charged (q = +1), whereas the q = +2 state is not stable because one electron is strongly bound by N_O. The neutral charge state is stable close to the CBM, with the (0/+1) CTL is 0.7 eV below the CBM, an energy similar to the corresponding one for the isolated OV. The negatively charged states (such as q = -1 or -2) of the defect complex are not stable. Rather, in the energetically favored config-

uration for q = -1, one electron is localized in proximity of the defect complex, and the other one forms as a small polaron in the bulk area of BVO, far from the defect.

In Figure 4, we also compare the DFE of OV, N_O, and OV-No in order to understand under which conditions (i.e., Fermi level position) OV and No form a defect complex, and under which conditions they are present as isolated defects. Focusing on the *n*-type region near the conduction band edge, we note that there are three distinctive conditions, defined by the position of the Fermi level and labeled as (1), (2), and (3). In a highly n-doped BVO, the Fermi level is expected to lie very close to the conduction band edge (see (3) in Figure 4). In such a case, the DFE of a negatively charged No is lower than that of the neutral OV, consistent with the previous experimental finding that BVO can be easily nitrogenated even with a very gentle N2 treatment. 17 In addition, the DFE of the OV-No pair is higher than the sum of the DFEs of isolated OV and No, indicating that the OV-No complex formation is not energetically preferred; hence in the region (3) OV and N_0 are stable as separate defects. Using the PBE +U functional (results are shown in Figure S5), we observe a qualitatively similar behavior.

However, when the Fermi level is within (2) in Figure 4, the formation of the $OV-N_O$ pair is favored as the DFE of the $OV-N_O$ pair is lower than the sum of the DFEs of the isolated OV and the isolated OV. In addition, in (2), the DFE of the isolated OV becomes comparable to that of the isolated OV, indicating that the equilibrium concentration of the two defects is expected to be similar. Thus, if the Fermi level lies within the region (2) of Figure 4, most of the OVs and the OV1 impurities would form $OV-N_O$ 1 complexes and the concentration of the isolated OV3 ion would be significantly reduced compared to the conditions described for (3) above.

Finally, if the Fermi level lies below (2) in Figure 4, i.e., within (1), the DFE of the N impurity significantly increases while the DFE of the OV decreases, indicating that the OV concentration would be much larger than that of the N impurity.³² Under these conditions, the stable charge state of the O vacancy is +1 and the corresponding donor level is the (+2/+1) CTL, which is calculated to be 1.14 (0.87) eV below the CBM using the DDH (PBE+U) functional. The ionization energy of the OV⁺ with respect to the polaron level of bulk BVO is computed to be 0.49 eV using the DDH functional, indicating that OV⁺ would not contribute to the charge concentration in BVO at room temperature.

In sum, we have shown that there are conditions (that we expect to be present experimentally), under which N impurities prefer to form OV-N_O defect complexes. However, an important result of our DFE calculations is that the (+1/0)CTL of the OV-N_O pair is almost the same as that of the isolated OV, indicating that the OV-N_O pair behaves in a manner similar to the OV, i.e., it may still act as a donor and contribute to donating polaronic charges to the material. Because it is known from experiments that the presence of N increases the OV concentration, ¹⁷ our results indicate that in the presence of nitrogen the carrier concentration in the material should increase, regardless of whether OV forms a complex with No. We have also shown that in the highly ndoped BVO, N impurities prefer to be present as isolated defects. We will show below that N impurities in isolated forms could contribute to enhancing the mobility of polaronic carriers in BVO by acting as polaronic repulsion centers.

3.4. Polaron Transport in the Presence of the Defects: CDFT Calculations. To investigate small polaron transport in the presence of defects (N impurities, OV and $OV-N_O$ pairs), we used CDFT to compute the hopping barrier W_H (eq 2). We considered a donor state (an electron polaron) localized at a V site (labeled as A in Figure 6) in the

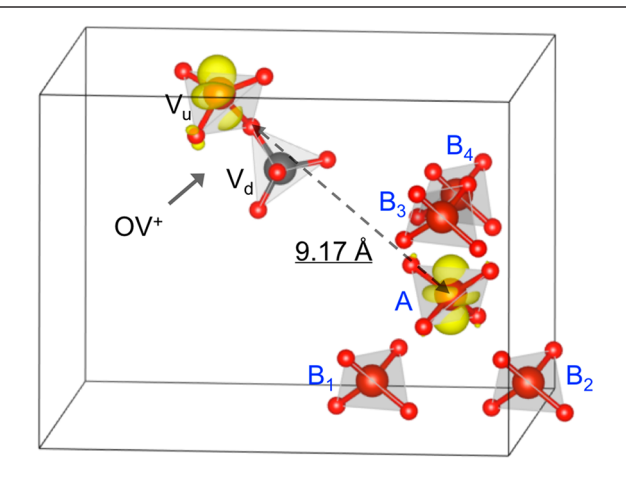


Figure 6. Representative, singly ionized oxygen vacancy (OV⁺) with donor and acceptor sites (see Figure 2) is shown on the left-hand side, together with one electron trapped at a bulk site (A), 9.17 Å apart from the vacancy. The four nearest neighbor sites where the trapped electron may hop are indicated as B1 to B4. The distances between the OV site and B1–B4 are 9.59 Å to B1, 10.39 Å to B2, 9.38 Å to B3, and 7.20 Å to B4.

bulk region of the supercell, at a distance of 9.17 Å from the ionized defect site (a defect site ionized once, labeled as V_u in Figure 6). We then considered all acceptor states localized at the nearest neighboring V sites of the donor atom (labeled as B1 to B4 in Figure 6); these represent the most probable hopping paths, assuming a small polaron hopping mechanism adopted at room temperature, since the barrier increases as a function of the hopping distance. (Note that at low temperature (<250 K) a variable-range hopping mechanism dominates and hopping beyond nearest neighbors should be considered 10). Figure 6 shows hopping from site A to nearest neighboring sites B1–B4 in the presence of singly ionized oxygen vacancy (OV⁺).

We consider the OV case first. In Table 1, we summarize the polaron hopping barriers computed in the presence of an OV⁺, i.e., a singly ionized oxygen vacancy, which can easily form based on our total energy calculations. Note that in our calculations the whole supercell is neutral when we consider a positively ionized vacancy and an electron polaron located far from the defect. In this case, we find that the hopping barriers are asymmetrical; namely, barriers along the A to B directions are slightly lower (30–50 meV) than those computed in the pristine case, whereas barriers along the B to A directions are higher. There are two possible reasons for this asymmetry: (a) the finite supercell size is not large enough to avoid periodic image interactions; (b) the defect-polaron interaction does not vanish as a function of distance in Figure 6. Therefore, the hopping sites are no longer equivalent in the presence of defects.

Therefore, we defined an effective barrier as the average of the barriers from A to B and from B to A. Table 1 shows that the overall average barrier for polaron hopping in the presence of OVs, 0.232 eV, is nearly the same as the one found in the

Table 1. Computed Hopping Barrier $W_{\rm H}$ (eV) for Pristine BVO, and for BVO with OV⁺ and OV-N_O⁺ Defect Configurations Shown in Figure 6^a

configuration	$W_{\rm H} \ (A { ightarrow} { m B})$	$W_{\rm H}~({\rm B}{ ightarrow}{ m A})$	W_{H} avg
pristine	0.238	0.238	0.238
OV $(A \rightarrow B1)$	0.189	0.281	0.235
OV $(A \rightarrow B2)$	0.180	0.280	0.230
OV $(A \rightarrow B3)$	0.191	0.264	0.227
OV $(A \rightarrow B4)$	0.207	0.267	0.237
OV avg	0.192	0.273	0.232
$OV-N_O (A \rightarrow B1)$	0.200	0.284	0.242
$OV-N_O (A \rightarrow B2)$	0.191	0.272	0.231
$OV-N_O (A \rightarrow B3)$	0.190	0.266	0.228
$OV-N_O (A \rightarrow B4)$	0.209	0.285	0.247
OV-N _O avg	0.197	0.276	0.236

^aThe results were obtained at the DDH level of theory. OV and No denote oxygen vacancy and nitrogen substitution of oxygen, respectively.

pristine oxide (0.238 eV). We note that we also computed the electron polaron hopping barrier in the presence of OV^0 (in this case the whole supercell is negatively charged), which is stable when the Fermi level is very close to CBM (regions (1) and (2)) in Figure 4); the hopping barriers differ by less than 10 meV from the ones evaluated in the presence of OV^+ . This result indicates that the bulk limit of hopping barriers is approximately recovered when an electron forms a polaron, at a distance larger than ~ 9 Å from the defect.

We also show the barrier $W_{\rm H}$ computed in the presence of the OV-N_O pair, 0.236 eV, which is almost identical to that computed for the OV, indicating again that at distances larger than 9 Å, the bulk limit is recovered.

We have shown in section 3.22. that if BVO is highly n-doped and the Fermi level lies close to the conduction band edge, e.g. in the region (3) of Figure 4, then neutral OVs and negatively charged $N_{\rm O}$ impurities (N^{3-}) may coexist without forming pairs. In Table 2, we compare the relative total energy

Table 2. Relative Total Energies (in eV) As a Function of Distances between Polaron Location and $N_0^{\ a}$

"The total energy of the configuration where the polaron is closest to $N_{\rm O}$ is set as the zero of energy. The results were obtained at the DDH level of theory. A lower energy is observed when the polaron is further apart from the N dopant, indicating a "repulsion interaction" between N dopants and polarons.

of a polaron as a function of the distance from a $N_{\rm O}$ impurity center, varying from 1.8 to 7.2 Å. We find that it is energetically favorable for a polaron to move further apart from a negatively charged $N_{\rm O}$ impurity, resulting in an effective repulsive interaction between the $N_{\rm O}$ defect and the polaron. Such an interaction may contribute to a mobility enhancement for polarons close to N impurities, although many other factors contribute to determining the value of the mobility. These results are consistent with our previous study carried out with a continuum dielectric medium approach, where we found a lowering of the polaron hopping barrier in the presence of N doping, because of the decrease in the static dielectric constant.

4. CONCLUSIONS

In summary, we showed that doping BVO with OVs and N impurities may significantly improve the carrier concentration and the carrier mobility in BVO. The donor level of the neutral OV is deep with respect to the conduction band edge, i.e., 0.76 eV (0.59 eV) below the CBM at 0K, when using the DDH (PBE+U) functional. We emphasize, however, that the deepstate character of the OV does not imply that the vacancy is not an effective source of charge carriers. In fact, the carrier transport in BVO at room temperature is dominated by small polaron transport, and we found that the ionization energy of the O vacancy can be less than 0.1 eV, with respect to the polaron level in the pristine material; this indicates that the localized electrons provided by an OV may be easily ionized (specifically one of these electrons can) and hence they contribute to polaron carriers and to the n-type character of the material. In addition, a recent theoretical work²⁰ showed at a finite temperature, the band gap and conduction band edge of BVO are significantly lowered relative to 0 K (i.e., the conduction band is lowered by 0.36 eV), implying a lower ionization energy of OV relative to the CBM relative to the one computed in our work. Hence the deep vacancy states are expected to become shallower at finite temperature and therefore contribute in an even more substantial way than at low temperature to polaronic conduction. However, a definite conclusion on temperature effects would require additional first-principles simulations, beyond the scope of the present

In the case of nitrogen doped BVO, we also found that in the highly n-doped material negatively charged N impurities have a very low defect formation energy, implying that they can be easily incorporated in BVO, providing an explanation for our previous findings; ¹⁷ indeed, in ref 17, we observed that nitrogen doping of BVO could be achieved by annealing BVO at 350 °C while flowing N_2 . This is an exceptionally gentle procedure considering that usual N doping of oxides requires much higher annealing temperature (>500 °C) with a flow of NH₂.

We analyzed the interplay between the N_O and OV defects by determining their ground-state structure (separate forms vs paired structure) using the defect formation energy for a given Fermi level of the material. However, additional factors not considered here may affect the formation of a defect complex, e.g., preparation conditions: A Fermi level shift might occur in the presence of unintended donors or acceptors and the defect diffusion may be facilitated or suppressed depending on the annealing temperature; considering these factors is beyond the scope of our study. For the OV defects, however, our main conclusion is robust against the shift of the Fermi level or defect kinetic properties: regardless of paring with No or not, OV could still act as a donor and contribute to donating polaronic charges to the material as the (+1/0) CTL of the pair is almost the same as that of the isolated OV, implying that the OV-N_O pair behaves in a manner similar to the OV.

We also note that N doping may create extra oxygen vacancies, as discussed in our previous study. ¹⁷ In addition, it may be also possible that N doping facilitates the inclusion of H donors into BVO as compensating defects. H atoms are often present in the material exposed to air and their concentration can be easily increased by a gentle treatment, as recently demonstrated in ref. ¹⁶

Our results for hopping barriers and total energies calculations as a function of the polaron-dopant distance showed that the effect of dopants/defects on the hopping barriers is rather short-ranged, i.e., the bulk limit is recovered at a polaron-dopant distance of ~ 9 Å. However, when polarons are formed in the proximity of dopants, a possible repulsive interaction may occur, for example, between N^{3-} and electron polarons, leading to an improvement of the carrier mobility. The same conclusion obtained here based on a microscopic picture was reached by using a macroscopic dielectric continuum model for the polaron hopping barriers in our previous work. 17

To conclude, we investigated the properties of point defects in BVO and their influence in determining the charge transport of the material. We used first-principles hybrid DFT and constrained DFT to examine the stability of O vacancies, N impurities, and their complexes. In particular, we focused on the interplay between the defects and the formation of small polarons, and we elucidated the microscopic mechanism responsible for enhanced carrier mobility and concentration of N-doped BVO with excessive O vacancies. Our study lays a solid foundation to understand the mechanisms responsible for point defects enhancing the conductivity of BVO, and in general for polaronic metal oxides.

ASSOCIATED CONTENT

S Supporting Information

The Supporting Information is available free of charge on the ACS Publications Web site. The Supporting Information is available free of charge on the ACS Publications website at DOI: 10.1021/acs.chemmater.8b03201.

Electronic structure of *n*-doped *ts*-BVO, total energy of a BVO crystal with an electron localized at a neutral oxygen vacancy, configurations of a positively charged oxygen vacancy, defect formation energies obtained with the PBE+U functional, electron localized at a substitutional nitrogen site, ground-state structure of a neutral oxygen vacancy-nitrogen dopant complex, and computed bulk properties of *ts*-BiVO₄ at the PBE, PBE+U, and DDH levels of theory (PDF)

AUTHOR INFORMATION

Corresponding Author

*E-mail: gagalli@uchicago.edu.

ORCID

Hosung Seo: 0000-0001-5677-111X Yuan Ping: 0000-0002-0123-3389

Author Contributions

[†]H.S. and Y.P. contributed equally.

Notes

The authors declare no competing financial interest.

ACKNOWLEDGMENTS

We thank Nicholas Brawand for many useful discussions on constrained density functional theory. H.S. was supported by the "New Faculty Research Fund" of Ajou University and by the National Research Foundation of Korea (NRF) grant funded by the Korea government (MSIT) (2018R1C1B6008980) after September 2017 and he was also supported by UChicago MRSEC before August 2017. Y.P. was supported by the National Science Foundation under

grant DMR-1760260 and the Hellman Fellowship. G.G. was supported by DOE-BES grant DE-FG02-06ER46262.

REFERENCES

- (1) Abdi, F.; Firet, N.; van de Krol, R. Efficient BiVO4 Thin Film Photoanodes Modified with Cobalt Phosphate Catalyst and Wdoping. *ChemCatChem* **2013**, *5*, 490–496.
- (2) Park, Y.; McDonald, K.; Choi, K. Progress in bismuth vanadate photoanodes for use in solar water oxidation. *Chem. Soc. Rev.* **2013**, 42, 2321–2337.
- (3) Sivula, K.; van de Krol, R. Semiconducting materials for photoelectrochemical energy conversion. *Nat. Rev. Mater.* **2016**, *1*, 15010.
- (4) Lee, D.; Choi, K. Enhancing long-term photostability of BiVO4 photoanodes for solar water splitting by tuning electrolyte composition. *Nat. Energy* **2018**, 3, 53–60.
- (5) Abdi, F.; Savenije, T.; May, M.; Dam, B.; van de Krol, R. The Origin of Slow Carrier Transport in BiVO4 Thin Film Photoanodes: A Time-Resolved Microwave Conductivity Study. *J. Phys. Chem. Lett.* **2013**, *4*, 2752–2757.
- (6) Butler, K.; Dringoli, B.; Zhou, L.; Rao, P.; Walsh, A.; Titov, L. Ultrafast carrier dynamics in BiVO4 thin film photoanode material: interplay between free carriers, trapped carriers and low-frequency lattice vibrations. *J. Mater. Chem. A* **2016**, *4*, 18516–18523.
- (7) Ziwritsch, M.; Muller, S.; Hempel, H.; Unold, T.; Abdi, F.; van de Krol, R.; Friedrich, D.; Eichberger, R. Direct Time-Resolved Observation of Carrier Trapping and Polaron Conductivity in BiVO4. ACS Energy Lett. 2016, 1, 888–894.
- (8) Jayah, N.; Yahaya, H.; Mahmood, M.; Terasako, T.; Yasui, K.; Hashim, A. High electron mobility and low carrier concentration of hydrothermally grown ZnO thin films on seeded alpha-plane sapphire at low temperature. *Nanoscale Res. Lett.* **2015**, *10*, 7.
- (9) Park, H.; Kweon, K.; Ye, H.; Paek, E.; Hwang, G.; Bard, A. Factors in the Metal Doping of BiVO4 for Improved Photoelectrocatalytic Activity as Studied by Scanning Electrochemical Microscopy and First-Principles Density-Functional Calculation. *J. Phys. Chem. C* 2011, *115*, 17870–17879.
- (10) Rettie, A.; Lee, H.; Marshall, L.; Lin, J.; Capan, C.; Lindemuth, J.; McCloy, J.; Zhou, J.; Bard, A.; Mullins, C. Combined Charge Carrier Transport and Photoelectrochemical Characterization of BiVO4 Single Crystals: Intrinsic Behavior of a Complex Metal Oxide. J. Am. Chem. Soc. 2013, 135, 11389–11396.
- (11) Seabold, J.; Zhu, K.; Neale, N. Efficient solar photoelectrolysis by nanoporous Mo: BiVO4 through controlled electron transport. *Phys. Chem. Chem. Phys.* **2014**, *16*, 1121–1131.
- (12) Jo, W.; Jang, J.; Kong, K.; Kang, H.; Kim, J.; Jun, H.; Parmar, K.; Lee, J. Phosphate Doping into Monoclinic BiVO4 for Enhanced Photoelectrochemical Water Oxidation Activity. *Angew. Chem., Int. Ed.* **2012**, *51*, 3147–3151.
- (13) Yin, W.; Wei, S.; Al-Jassim, M.; Turner, J.; Yan, Y. Doping properties of monoclinic BiVO4 studied by first-principles density-functional theory. *Phys. Rev. B: Condens. Matter Mater. Phys.* **2011**, 83, 155102.
- (14) Wang, G.; Ling, Y.; Lu, X.; Qian, F.; Tong, Y.; Zhang, J.; Lordi, V.; Rocha Leao, C.; Li, Y. Computational and Photoelectrochemical Study of Hydrogenated Bismuth Vanadate. *J. Phys. Chem. C* **2013**, *117*, 10957–10964.
- (15) Jang, J.; Friedrich, D.; Muller, S.; Lamers, M.; Hempel, H.; Lardhi, S.; Cao, Z.; Harb, M.; Cavallo, L.; Heller, R.; Eichberger, R.; van de Krol, R.; Abdi, F. Enhancing Charge Carrier Lifetime in Metal Oxide Photoelectrodes through Mild Hydrogen Treatment. *Adv. Energy Mater.* **2017**, *7*, 1701536.
- (16) Cooper, J.; Scott, S.; Ling, Y.; Yang, J.; Hao, S.; Li, Y.; Toma, F.; Stutzmann, M.; Lakshmi, K.; Sharp, I. Role of Hydrogen in Defining the n-Type Character of BiVO4 Photoanodes. *Chem. Mater.* **2016**, 28, 5761–5771.
- (17) Kim, T.; Ping, Y.; Galli, G.; Choi, K. Simultaneous enhancements in photon absorption and charge transport of bismuth

vanadate photoanodes for solar water splitting. Nat. Commun. 2015, 6, 8769

- (18) Janotti, A.; Varley, J.; Choi, M.; van de Walle, C. Vacancies and small polarons in SrTiO3. *Phys. Rev. B: Condens. Matter Mater. Phys.* **2014**, *90*, 085202.
- (19) Miceli, G.; Chen, W.; Reshetnyak, I.; Pasquarello, A. Nonempirical hybrid functionals for band gaps and polaronic distortions in solids. *Phys. Rev. B: Condens. Matter Mater. Phys.* **2018**, 97, 121112.
- (20) Wiktor, J.; Reshetnyak, I.; Ambrosio, F.; Pasquarello, A. Comprehensive modeling of the band gap and absorption spectrum of BiVO4. *Phys. Rev. Mater.* **2017**, *1*, 022401.
- (21) Giannozzi, P.; Baroni, S.; Bonini, N.; Calandra, M.; Car, R.; Cavazzoni, C.; Ceresoli, D.; Chiarotti, G.; Cococcioni, M.; Dabo, I.; Dal Corso, A.; de Gironcoli, S.; Fabris, S.; Fratesi, G.; Gebauer, R.; Gerstmann, U.; Gougoussis, C.; Kokalj, A.; Lazzeri, M.; Martin-Samos, L.; Marzari, N.; Mauri, F.; Mazzarello, R.; Paolini, S.; Pasquarello, A.; Paulatto, L.; Sbraccia, C.; Scandolo, S.; Sclauzero, G.; Seitsonen, A.; Smogunov, A.; Umari, P.; Wentzcovitch, R. QUANTUM ESPRESSO: a modular and open-source software project for quantum simulations of materials. *J. Phys.: Condens. Matter* **2009**, *21*, 395502.
- (22) Hamann, D. Optimized norm-conserving Vanderbilt pseudo-potentials. *Phys. Rev. B: Condens. Matter Mater. Phys.* **2013**, 88, 085117.
- (23) Schlipf, M.; Gygi, F. Optimization algorithm for the generation of ONCV pseudopotentials. *Comput. Phys. Commun.* **2015**, *196*, 36–44.
- (24) Skone, J.; Govoni, M.; Galli, G. Self-consistent hybrid functional for condensed systems. *Phys. Rev. B: Condens. Matter Mater. Phys.* **2014**, *89*, 195112.
- (25) Dudarev, S.; Botton, G.; Savrasov, S.; Humphreys, C.; Sutton, A. Electron-energy-loss spectra and the structural stability of nickel oxide: An LSDA+U study. *Phys. Rev. B: Condens. Matter Mater. Phys.* 1998, *57*, 1505–1509.
- (26) Sleight, A.; Chen, H.; Ferretti, A.; Cox, D. Crystal-growth and structure of BiVO4. *Mater. Res. Bull.* 1979, 14, 1571–1581.
- (27) Payne, D.; Robinson, M.; Egdell, R.; Walsh, A.; McNulty, J.; Smith, K.; Piper, L. The nature of electron lone pairs in BiVO4. *Appl. Phys. Lett.* **2011**, *98*, 212110.
- (28) Stoughton, S.; Showak, M.; Mao, Q.; Koirala, P.; Hillsberry, D.; Sallis, S.; Kourkoutis, L.; Nguyen, K.; Piper, L.; Tenne, D.; Podraza, N.; Muller, D.; Adamo, C.; Schlom, D. Adsorption-controlled growth of BiVO4 by molecular-beam epitaxy. *APL Mater.* **2013**, *1* (4), 042112.
- (29) Cooper, J.; Gul, S.; Toma, F.; Chen, L.; Glans, P.; Guo, J.; Ager, J.; Yano, J.; Sharp, I. Electronic Structure of Monoclinic BiVO4. *Chem. Mater.* **2014**, *26*, 5365–5373.
- (30) Cooper, J.; Gul, S.; Toma, F.; Chen, L.; Liu, Y.; Guo, J.; Ager, J.; Yano, J.; Sharp, I. Indirect Bandgap and Optical Properties of Monoclinic Bismuth Vanadate. *J. Phys. Chem. C* **2015**, *119*, 2969–2974.
- (31) Kweon, K.; Hwang, G. Hybrid density functional study of the structural, bonding, and electronic properties of bismuth vanadate. *Phys. Rev. B: Condens. Matter Mater. Phys.* **2012**, *86*, 165209.
- (32) Freysoldt, C.; Neugebauer, J.; Van de Walle, C. Fully Ab Initio Finite-Size Corrections for Charged-Defect Supercell Calculations. *Phys. Rev. Lett.* **2009**, *102*, 016402.
- (33) Adelstein, N.; Neaton, J.; Asta, M.; De Jonghe, L. Density functional theory based calculation of small-polaron mobility in hematite. *Phys. Rev. B: Condens. Matter Mater. Phys.* **2014**, 89, 245115.
- (34) Austin, I.; Mott, N. Polarons in crystalline and non-crystalline materials. *Adv. Phys.* **2001**, *50*, 757–812.
- (35) Deskins, N.; Dupuis, M. Electron transport via polaron hopping in bulk TiO2: A density functional theory characterization. *Phys. Rev. B: Condens. Matter Mater. Phys.* **2007**, *75*, 195212.
- (36) Holstein, T. Studies of polaron motion Part I. The molecular-crystal model (Reprinted from Annals of Physics, vol 8, pg 325–342, 1959). *Ann. Phys.* **2000**, 281, 706–724.

(37) Rettie, A.; Chemelewski, W.; Emin, D.; Mullins, C. Unravelling Small-Polaron Transport in Metal Oxide Photoelectrodes. *J. Phys. Chem. Lett.* **2016**, *7*, 471–479.

- (38) Blumberger, J.; McKenna, K. Constrained density functional theory applied to electron tunnelling between defects in MgO. *Phys. Chem. Chem. Phys.* **2013**, *15*, 2184–2196.
- (39) Oberhofer, H.; Blumberger, J. Revisiting electronic couplings and incoherent hopping models for electron transport in crystalline C-60 at ambient temperatures. *Phys. Chem. Chem. Phys.* **2012**, *14*, 13846–13852.
- (40) Marcus, R. A. Electron-transfer Reactions in Chemistry-Theory and Experiment. *Rev. Mod. Phys.* **1993**, *65*, 599–610.
- (41) Goldey, M.; Brawand, N.; Voros, M.; Galli, G. Charge Transport in Nanostructured Materials: Implementation and Verification of Constrained Density Functional Theory. *J. Chem. Theory Comput.* **2017**, *13*, 2581–2590.
- (42) Kweon, K.; Hwang, G.; Kim, J.; Kim, S.; Kim, S. Electron small polarons and their transport in bismuth vanadate: a first principles study. *Phys. Chem. Chem. Phys.* **2015**, *17*, 256–260.
- (43) Plata, J.; Marquez, A.; Sanz, J. Electron Mobility via Polaron Hopping in Bulk Ceria: A First-Principles Study. *J. Phys. Chem. C* **2013**, *117*, 14502–14509.
- (44) Liao, P.; Toroker, M.; Carter, E. Electron Transport in Pure and Doped Hematite. *Nano Lett.* **2011**, *11*, 1775–1781.